Optics Letters

Wide-angle polarization selectivity based on anomalous defect mode in photonic crystal containing hyperbolic metamaterials

FENG WU,[1,*] MINGYUAN CHEN,[2] AND SHUYUAN XIAO[3,4]

[1]School of Optoelectronics and Engineering, Guangdong Polytechnic Normal University, Guangzhou 510665, China
[2]Materials Research and Education Center, Department of Mechanical Engineering, Auburn University, Alabama 36849, USA
[3]Institute for Advanced Study, Nanchang University, Nanchang 330031, China
[4]Jiangxi Key Laboratory for Microscale Interdisciplinary Study, Nanchang University, Nanchang 330031, China
*Corresponding author: fengwu@gpnu.edu.cn

Received 11 February 2022; accepted 23 March 2022; posted 25 March 2022; published 19 April 2022

Conventional defect modes in all-dielectric 1D photonic crystals (PCs) are polarization-insensitive. This poses a great challenge in achieving high-performance polarization selectivity. In this Letter, we introduce a defect layer into a 1D PC containing hyperbolic metamaterials to achieve an *anomalous* defect mode with polarization-sensitive characteristics. As the incident angle increases, such a defect mode remains almost unshifted under transverse magnetic polarization, while strongly shifting toward shorter wavelengths under transverse electric polarization. The polarization-sensitive characteristics of the defect mode can be well explained by the Fabry–Perot resonance condition. Assisted by the polarization-sensitive defect mode, wide-angle polarization selectivity with an operating angle width up to 54.8° can be realized. Our work provides a route to designing wide-angle linear polarizers using simple 1D structures, which would be useful in liquid crystal display and *Q*-switched lasers.

https://doi.org/10.1364/OL.455910

By introducing defects into photonic crystals (PCs), types of resonant mode called defect modes will emerge within photonic band gaps (PBGs) [1]. Over the past two decades, defect modes have been widely utilized in filters [2], fibers [3], and nonlinear devices [4]. In particular, defect modes in all-dielectric one-dimensional (1D) PCs have received enormous attention, since all-dielectric 1D PCs are easily fabricated [5–8]. However, it is known that defect modes in all-dielectric 1D PCs are polarization-insensitive [9,10]. Under both transverse magnetic (TM) and transverse electric (TE) polarizations, defect modes in all-dielectric 1D PCs will shift toward shorter wavelengths (i.e., blueshift) as the incident angle increases [9,10]. The underlying physics can be demonstrated as follows. According to the multiple-interference mechanism, PBGs in all-dielectric 1D PCs shift toward shorter wavelengths as the incident angle increases under both TM and TE polarizations [11–14]. Hence, the reflection phase at a fixed wavelength within the PBG decreases. Besides, the propagating phase within the defect layer at a fixed wavelength also decreases under both TM and TE polarizations, since the perpendicular component of the wave vector decreases. As a result, when the incident angle increases, the total phase accumulated during a single round trip in a defective 1D PC at a fixed wavelength decreases and then the wavelength satisfying the Fabry–Perot resonance condition decreases. In other words, defect modes will shift toward shorter wavelengths under both TM and TE polarizations [9,10]. The polarization-insensitive characteristic of defect modes in all-dielectric 1D PCs poses a great challenge in achieving high-performance polarization selectivity [9,10]. A numerical example is presented in Section 1 of Supplement 1 to confirm this phenomenon. In the past few decades, researchers have proposed various mechanisms to realize wide-angle polarization selectivity in microstructures [15–21]. However, the question of how to achieve wide-angle polarization selectivity based on defect modes in 1D PCs is still an open problem.

Recently, hyperbolic metamaterials (HMMs) attracted great interest since they demonstrate unique optical properties that are not found in natural materials [22–24]. Interestingly, they can support high-k modes, owing to their hyperbolic isofrequency surfaces [25]. In 2014, Narimanov theoretically proposed a new class of artificial periodic optical media called photonic hypercrystals [26]. Such optical media contain alternating HMMs and dielectrics (or metals) on the subwavelength scale. Hence, they combine the features of optical metamaterials and PCs, giving rise to potential applications in controlling surface waves [26], spontaneous emission [27,28], and nonlinear optical processes [29,30]. The first experimental demonstration of photonic hypercrystals was reported the next year [31]. In addition, researchers proposed a special type of 1D PC, which contains alternating HMMs and dielectrics on the wavelength scale to engineer PBGs [32–34]. Such 1D PCs can be called 1D PCs containing HMMs (PCCHs). In particular, researchers achieved a new class of PBG, called a redshift PBG, in 1D PCCHs under TM polarization [35]. Fully distinctive from conventional blueshift PBGs in all-dielectric 1D PCs, redshift PBGs in 1D PCCHs shift toward longer wavelengths as the incident angle increases under TM polarization. Hence, it can be expected that the reflection phase at a fixed wavelength within the redshift PBG will increase, in contrast with the blueshift PBG. However, under TE

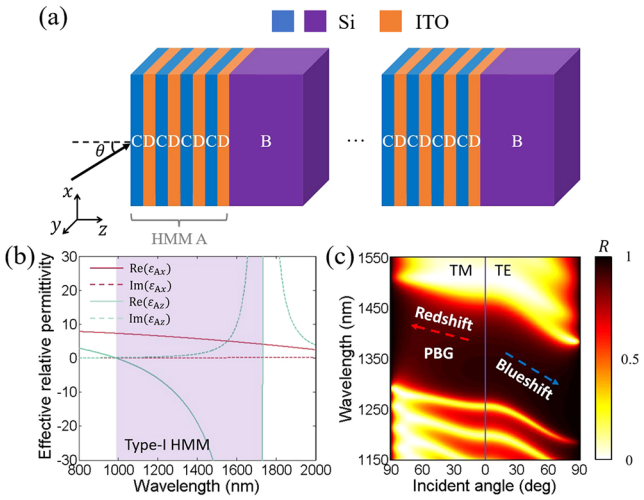

Fig. 1. (a) 1D PCCH. The HMM layer is mimicked by a subwavelength Si–ITO multilayer $(CD)^4$. The whole structure can be denoted $[(CD)^4B]^{12}$. (b) Two components of the effective relative permittivity tensor of the subwavelength Si–ITO multilayer $(CD)^4$ as a function of the wavelength. (c) Reflectance spectrum of the structure $[(CD)^4B]^{12}$ as a function of the incident angle under TM and TE polarizations.

polarization, this type of PBG is blueshifted like conventional PBGs, giving rise to a decrease in the reflection phase at a fixed wavelength within the PBG [35]. Such polarization-dependent behavior of the reflection phase in 1D PCCHs offers a feasibility to realize a polarization-sensitive defect mode.

In this Letter, we introduce a dielectric defect layer into a 1D PCCH to realize an *anomalous* defect mode with polarization-sensitive characteristic. Under TM polarization, as the incident angle increases, the reflection phase of the 1D PCCH at a fixed wavelength within the redshifted PBG increases, while the propagating phase within the dielectric defect layer at a fixed wavelength decreases. Therefore, the defect mode can be designed to be angle-insensitive. Under TE polarization, as the incident angle increases, the reflection phase of the 1D PCCH at a fixed wavelength within the blueshifted PBG decreases. Hence, the defect mode becomes blueshifted. Assisted by the designed *anomalous* defect mode in the 1D PCCH, we achieve wide-angle polarization selectivity. Our work provides a route to designing wide-angle linear polarizers using simple 1D structures.

To realize a polarization-sensitive defect mode in a 1D PCCH, a redshifted PBG in a 1D PCCH under TM polarization should be designed. Now we design a redshifted PBG based on the theory in Ref. [35]. The 1D PCCH is composed of alternating HMM layers (A layers) and dielectric layers (B layers), as shown schematically in Fig. 1(a). The HMM layer is mimicked by a subwavelength silicon (Si)–indium tin oxide (ITO) multilayer $(CD)^4$ and the dielectric layer is a Si layer. The whole structure can be denoted $[(CD)^4B]^{12}$. The refractive index of Si is 3.48 [36]. ITO is a widely used plasmonic material at near-infrared wavelengths, whose relative permittivity can be described by the Drude model [37]:

$$\varepsilon_D = \varepsilon_{inf} - \frac{\omega_P^2}{\omega^2 + i\gamma\omega}, \tag{1}$$

where ε_{inf}, ω_P, ω, and γ represent the high-frequency permittivity, the plasma angular frequency, the angular frequency, and the damping angular frequency, respectively. The values of the parameters $\varepsilon_{inf} = 3.9$, $\hbar\omega_P = 2.48$ eV, and $\hbar\gamma = 0.016$ eV can be fitted by experimental measurement [37]. According to the effective medium theory, two components of the effective relative permittivity tensor of the subwavelength Si–ITO multilayer $(CD)^4$ can be determined by [22]

$$\varepsilon_{Ax} = f\varepsilon_C + (1-f)\varepsilon_D, \tag{2}$$

$$\frac{1}{\varepsilon_{Az}} = \frac{f}{\varepsilon_C} + \frac{1-f}{\varepsilon_D}, \tag{3}$$

where $f = d_C/(d_C + d_D)$ represents the filling ratio of the Si layer. In our design, we choose $f = 0.6$. Figure 1(b) gives two components of the effective relative permittivity tensor as a function of the wavelength. One can see that $\mathrm{Re}(\varepsilon_{Ax}) > 0$ and $\mathrm{Re}(\varepsilon_{Az}) < 0$ are satisfied within the wavelength range from 990 nm to 1733 nm (so-called type-I hyperbolic region), which indicates that the subwavelength Si–ITO multilayer $(CD)^4$ can be viewed as a type-I HMM layer.

It is known that the Bragg condition of the lowest-frequency PBG can be given by [38]

$$\Phi = (k_{Az}d_A + k_{Bz}d_B)|_{\lambda_{Brg}} = \pi, \tag{4}$$

where Φ represents the propagating phase within a unit cell, k_{Az} (k_{Bz}) represents the z component of the wave vector within the HMM layer (the dielectric layer), and λ_{Brg} represents the Bragg wavelength. To obtain a redshifted PBG under TM polarization, the following condition should be satisfied:

$$\frac{\partial\Phi}{\partial k_x} = \left(\frac{\partial k_{Az}}{\partial k_x}d_A + \frac{\partial k_{Bz}}{\partial k_x}d_B\right)\Big|_{\lambda_{Brg}} > 0, \tag{5}$$

where k_x represents the x component of the wave vector. After some derivations (see Ref. [35]), we can finally obtain two analytical conditions of the thicknesses of the HMM layer and the dielectric layer:

$$d_A > d_{Amin} = \frac{\lambda_{Brg}}{2}\frac{1}{\sqrt{Re(\varepsilon_{Ax})}[1 - \varepsilon_B/Re(\varepsilon_{Az})]}, \tag{6}$$

$$d_B = \frac{(\lambda_{Brg}/2) - \sqrt{Re(\varepsilon_{Ax})}d_A}{\sqrt{\varepsilon_B}}. \tag{7}$$

In our design, the Bragg wavelength is set to be $\lambda_{Brg} = 1350$ nm. From Eq. (6), we can obtain the minimum thickness of the HMM layer, $d_{Amin} = 150.5$ nm. We select the thickness of the HMM layer, $d_A = 210$ nm, and obtain the thickness of the dielectric layer, $d_B = 47.1$ nm, from Eq. (7). The thicknesses of the subwavelength Si and ITO layers are $d_C = fd_A/4 = 31.5$ nm and $d_D = (1-f)d_A/4 = 21$ nm, respectively. Based on the transfer matrix method [39], we calculate the reflectance spectrum of the 1D PCCH $[(DE)^4B]^{12}$ as a function of the incident angle under TM and TE polarizations, as shown in Fig. 1(c). The incident medium is air and the exit medium (substrate) is BK7 glass with a refractive index of 1.515 [40]. One can see that, under TM polarization, the PBG shifts toward longer wavelengths as the incident angle increases. However, under TE polarization, the PBG shifts toward shorter wavelengths as the incident angle increases. Therefore, a redshifted PBG under TM polarization and a blueshifted PBG under TE polarization in a 1D PCCH are achieved.

Then, we introduce a dielectric defect layer into the designed 1D PCCH, $(AB)^{12}$, to realize an *anomalous* defect mode with

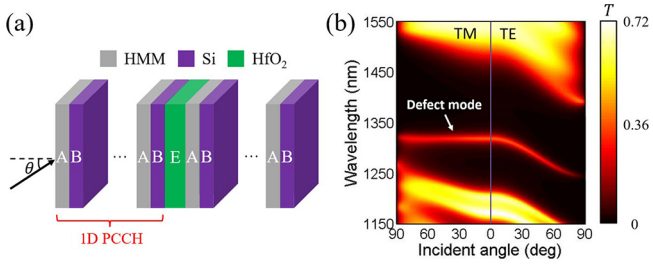

Fig. 2. (a) Designed 1D PCCH with dielectric defect layer. The whole structure can be denoted $(AB)^6E(AB)^6$, where $(AB)^{12}$ is the previously designed 1D PCCH and E is a dielectric (HfO_2) defect layer. (b) Transmittance spectrum of the structure $(AB)^6E(AB)^6$ as a function of the incident angle under TM and TE polarizations.

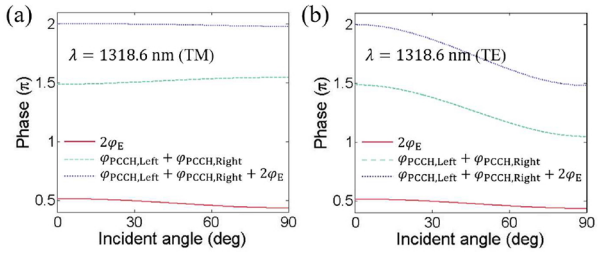

Fig. 3. Phase as a function of the incident angle at the wavelength of the defect mode ($\lambda = 1318.6$ nm) under (a) TM and (b) TE polarizations.

polarization-sensitive characteristics. As shown schematically in Fig. 2(a), the whole structure can be denoted $(AB)^6E(AB)^6$, where $(AB)^6$ is the previously designed 1D PCCH and E is a hafnium dioxide (HfO_2) defect layer with a refractive index of 1.88 [41]. The HMM layer (A layer) is mimicked by the previous Si/ITO multilayer $(CD)^4$. To realize an angle-insensitive defect mode under TM polarization, the thickness of the defect layer is set as $d_E = 90$ nm. We calculate the transmittance spectrum of the structure $(AB)^6E(AB)^6$ as a function of the incident angle under TM and TE polarizations, as shown in Fig. 2(b). The incident medium is air and the exit medium (substrate) is BK7 glass. One can see that under TM polarization, the wavelength of the defect mode is almost unshifted (around 1319 nm) as the incident angle increases from 0° to near 90°. However, under TE polarization, the defect mode shifts strongly toward shorter wavelengths as the incident angle increases from 0° to near 90°. We achieve a polarization-sensitive defect mode in a 1D PCCH, which can be further utilized to realize wide-angle polarization selectivity.

Next, we explain the polarization-sensitive characteristic of the defect mode based on the Fabry–Perot resonance condition. A defect mode will emerge when the Fabry–Perot resonance condition is satisfied, i.e.,

$$\varphi_{PCCH,Left} + 2\varphi_E + \varphi_{PCCH,Right} = 2m\pi (m = 0, 1, \ldots). \quad (8)$$

Here $\varphi_{PCCH,Left}$ ($\varphi_{PCCH,Right}$) represents the reflection phase from the defect layer to the left (right) 1D PCCH, and $2\varphi_E = 2k_{E_z}d_E$ represents the round-trip propagating phase within the defect layer. The single round-trip propagating phase within the defect layer $2\varphi_E$ can be further expanded as

$$2\varphi_E = 2k_{E_z}d_E = 2k_0\sqrt{n_E^2 - \sin^2\theta}, \quad (9)$$

where θ represents the incident angle. It should be noted that the reflection phases from the defect layer to the left 1D PCCH $\varphi_{PCCH,Left}$ and to the right 1D PCCH $\varphi_{PCCH,Right}$ are dependent on the polarization while the round-trip propagating phase within the defect layer $2\varphi_E$ is independent of the polarization. As shown by the solid lines in Fig. 3, as the incident angle increases from 0° to near 90°, the single round-trip propagating phase within the defect layer ($2\varphi_E$) at $\lambda = 1318.6$ nm under TM polarization decreases from 0.513π to 0.435π. As shown by the dashed line in Fig. 3(a), as the incident angle increases from 0° to near 90°, the sum of the reflection phases from the defect layer to the left 1D PCCH and to the right 1D PCCH ($\varphi_{PCCH,Left} + \varphi_{PCCH,Right}$) at $\lambda = 1318.6$ nm under TM polarization increases from 1.487π to 1.546π, owing to the redshift of the PBG [see Fig. 1(c)]. Therefore, the total phase accumulated during a single round trip ($\varphi_{PCCH,Left} + 2\varphi_E + \varphi_{PCCH,Right}$) at $\lambda = 1318.6$ nm under TM polarization remains around 2π at any incident angle, as shown by the dotted line in Fig. 3(a). In other words, the Fabry–Perot resonance condition can be almost satisfied at $\lambda = 1318.6$ nm at any incident angle under TM polarization, leading to an angle-insensitive defect mode under TM polarization. However, the situation is quite different under TE polarization. As shown by the dashed line in Fig. 3(b), as the incident angle increases from 0° to near 90°, the sum of the reflection phases from the defect layer to the left 1D PCCH and to the right 1D PCCH ($\varphi_{PCCH,Left} + \varphi_{PCCH,Right}$) at $\lambda = 1318.6$ nm under TE polarization decreases from 1.487π to 1.047π, owing to the blueshift of the PBG [see Fig. 1(c)]. Therefore, the total phase accumulated during a single round trip ($\varphi_{PCCH,Left} + 2\varphi_E + \varphi_{PCCH,Right}$) at $\lambda = 1318.6$ nm under TE polarization decreases from 2.000π to 1.481π, as shown by the dotted line in Fig. 3(b). To maintain the Fabry–Perot resonance condition, the wavelength must decrease. Hence, the wavelength of the defect mode becomes blueshifted under TE polarization.

Finally, we utilize the polarization-sensitive defect mode to realize wide-angle polarization selectivity. Figure 4(a) gives the transmittance at the wavelength of the defect mode ($\lambda = 1318.6$ nm) as a function of the incident angle under TM and TE polarizations. As the incident angle increases from 0° to 72°, the transmittance under TM polarization T^{TM} always remains at a relatively high level (around 0.3), since the defect mode remains around 1318.6 nm. It should be noted that the transmittance under TM polarization is not too high, owing to the absorption within the HMM layers. However, as the incident angle increases from 0°, the transmittance under TE polarization T^{TE} rapidly decreases since the defect mode shifts from 1318.6 nm to shorter wavelengths. Figure 4(b) gives the corresponding polarization selection ratio $\rho = T^{TM}/T^{TE}$. As the incident angle increases from

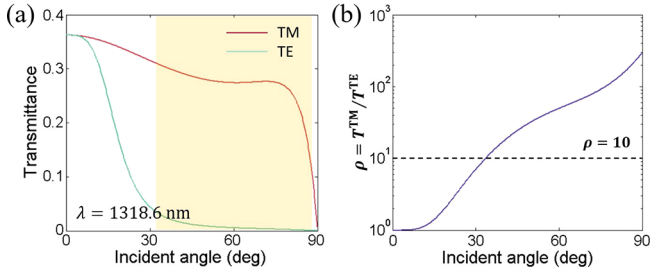

Fig. 4. (a) Transmittance at wavelength of defect mode ($\lambda = 1318.6$ nm) as a function of incident angle under TM and TE polarizations. (b) Corresponding polarization selection ratio.

0° to near 90°, the polarization selection ratio rapidly increases from 10° to over 3×10^2. Simultaneously considering the polarization selection ratio and the transmittance, we define the angle region where $\rho > 10$ and $T^{TM} > 0.1$ as the efficient polarization selectivity region. As shown by the shaded region in Fig. 4(a), the efficient polarization selectivity region ranges from 33.4° to 88.2°. The operating angle width of polarization selectivity reaches 54.8°. It should be noted that the performance of polarization selectivity is determined by the absorption within the HMM layers (see Section 2 of Supplement 1). The performance of polarization selectivity would be further improved when another epsilon-negative material with a lower loss is fabricated in the future.

In summary, we propose an *anomalous* defect mode with polarization-sensitive characteristic in a 1D PCCH. As the incident angle increases, the defect mode remains almost unshifted under TM polarization, while strongly shifting toward shorter wavelengths under TE polarization. Assisted by the polarization-sensitive defect mode, we achieve wide-angle polarization selectivity with an operating angle width up to 54.8°. These results would be helpful for the design of high-performance linear polarizers in liquid crystal displays [42] and Q-switched lasers [43].

Funding. National Natural Science Foundation of China (12104105; 11947065); Natural Science Foundation of Jiangxi Province (20202BAB211007); Interdisciplinary Innovation Fund of Nanchang University (2019-9166-27060003); Start-up Funding of Guangdong Polytechnic Normal University (2021SDKYA033).

Disclosures. The authors declare no conflicts of interest.

Data availability. Data underlying the results presented in this paper are not publicly available at this time but may be obtained from the authors upon reasonable request.

Supplemental document. See Supplement 1 for supporting content.

REFERENCES

1. Y. Akahane, T. Asano, B. Song, and S. Noda, Nature **425**, 944 (2003).
2. I. V. Timofeev, D. N. Maksimov, and A. F. Sadreev, Phys. Rev. B **97**, 024306 (2018).
3. S. Schuler, D. Schall, D. Neumaier, B. Schawarz, K. Watanabe, T. Taniguchi, and T. Mueller, ACS Photonics **5**, 4758 (2018).
4. Y. Xu, B. Wan, Z. Zhou, H. Zhang, and D. Zhang, Appl. Phys. B **127**, 101 (2021).
5. F. Qiao, C. Zhang, J. Wan, and J. Zi, Appl. Phys. Lett. **77**, 3698 (2000).
6. S. Guo, Z. Li, F. Li, Y. Xu, and H. Zhang, J. Appl. Phys. **129**, 093104 (2021).
7. L. Zhao, Y. Zhou, and A. Wang, Opt. Lett. **43**, 5387 (2018).
8. K. Huang, L. Cao, P. Zhai, P. Liu, L. Cheng, and J. Liu, Opt. Commun. **470**, 125392 (2020).
9. A. H. Aly and H. A. Elsayed, Phys. B **407**, 120 (2012).
10. G. Du, X. Zhou, C. Peng, K. Zhang, Y. Zhao, G. Lu, F. Liu, A. Wu, S. Akhmadaliev, S. Zhou, and F. Chen, Adv. Opt. Mater. **8**, 2000426 (2020).
11. Y. Fink, J. N. Winn, S. Fan, C. Chen, J. Michel, J. D. Joannopoulos, and E. L. Thomas, Science **282**, 1679 (1998).
12. X. Kong, S. Liu, H. Zhang, C. Li, and B. Bian, J. Opt. **13**, 035101 (2011).
13. Y. Zhang, Z. Wu, Y. Cao, and H. Zhang, Opt. Commun. **338**, 168 (2015).
14. D. Qi, F. Chen, X. Wang, H. Luo, Y. Cheng, X. Niu, and R. Gong, Opt. Lett. **43**, 5323 (2018).
15. L. Li and J. A. Dobrowolski, Appl. Opt. **35**, 2221 (1996).
16. L. Li and J. A. Dobrowolski, Appl. Opt. **39**, 2754 (2000).
17. L. Li, Opt. Photonics News **14**, 24 (2003).
18. S. K. Awasthi, A. Srivastava, U. Malaviya, and S. P. Ojha, Solid State Commun. **146**, 506 (2008).
19. S. K. Awasthi, A. Mishra, U. Malaviya, and S. P. Ojha, Solid State Commun. **149**, 1379 (2009).
20. Q. Hong, W. Xu, J. Zhang, Z. Zhu, X. Yuan, and S. Qin, Opt. Lett. **44**, 1774 (2019).
21. Y. Liang, H. Lin, K. Koshelev, F. Zhang, Y. Yang, J. Wu, Y. Kivshar, and B. Jia, Nano Lett. **21**, 1090 (2021).
22. L. Ferrari, C. Wu, D. Lepage, X. Zhang, and Z. Liu, Prog. Quantum Electron. **40**, 1 (2015).
23. B. Janaszek and P. Szczepański, Materials **14**, 4065 (2021).
24. F. Wu, X. Wu, S. Xiao, G. Liu, and H. Li, Opt. Express **29**, 23976 (2021).
25. M. Mahmoodi, S. H. Tavassoli, O. Takayama, J. Sukham, R. Malureanu, and A. L. Lavrinenko, Laser Photonics Rev. **13**, 1800253 (2019).
26. E. E. Narimanov, Phys. Rev. X **4**, 041014 (2014).
27. T. Galfsky, Z. Sun, C. R. Considine, C. Chou, W. Ko, E. E. Narimanov, and V. M. Menon, Nano Lett. **16**, 4940 (2016).
28. T. Galfsky, J. Gu, E. E. Narimanov, and V. M. Menon, P. Natl. Acad. Sci. USA **114**, 5125 (2017).
29. I. I. Smolyaninov, J. Opt. Soc. Am. B **36**, 1629 (2019).
30. M. Z. Ali, Phys. Lett. A **387**, 127026 (2021).
31. V. N. Smolyaninova, B. Yost, D. Lahneman, E. E. Narimanov, and I. I. Smolyaninov, Sci. Rep. **4**, 5706 (2015).
32. S. V. Zhukovsky, A. A. Orlov, V. E. Babicheva, A. V. Lavrinenko, and J. E. Sipe, Phys. Rev. A **90**, 013801 (2014).
33. J. Xia, Y. Chen, and Y. Xiang, Opt. Express **29**, 12160 (2021).
34. F. Wu, K. Lyu, S. Hu, M. Yao, and S. Xiao, Opt. Mater. **111**, 110680 (2021).
35. F. Wu, G. Lu, Z. Guo, H. Jiang, C. Xue, M. Zheng, C. Chen, G. Du, and H. Chen, Phys. Rev. Appl. **10**, 064022 (2018).
36. E. Palik, *Handbook of Optical Constants of Solids* (Academic, 1998).
37. T. Gerfin and M. Grätzel, J. Appl. Phys. **79**, 1722 (1996).
38. J. Li, L. Zhou, C. T. Chan, and P. Sheng, Phys. Rev. Lett. **90**, 083901 (2003).
39. P. Yeh, *Optical Waves in Layered Media* (Wiley, 1988).
40. L. Dominici, F. Michelotti, T. M. Brown, A. Reale, and A. D. Carlo, Opt. Express **17**, 10155 (2009).
41. M. F. Al-Kuhaili, Opt. Mater. **27**, 383 (2004).
42. C. Tsai and S. Wu, Appl. Opt. **47**, 2882 (2008).
43. J. Yang, L. Wang, X. Wu, T. Cheng, and H. Jiang, Opt. Express **22**, 15686 (2014).